Characterization of European Medieval Silver Bars Using Micro X-ray Fluorescence, Conductivity Meter and Scanning Electron Microscopy

Ahmad Nizamedien Barzingi

Department of Chemistry, College of Education, University of Garmian, University in Kalar, Iraq

A B S T R A C T

The objective of this paper is to use μ-X-ray fluorescence (XRF) analysis to evaluate the fineness and components of European Medieval Silver Bars samples. Conductivity measurements were used to assess the fineness and localization of the faults found in the samples. Because unevenness causes a change in conductivity, the tests were performed on the flattest areas of the Bars. Some rods, such as B3 and B9, have greater conductivity than others. All bars were subjected to the segregation test. In the instance of certain bars, it was not always practicable to categorically state that segregation had happened. There is no diminishing conductivity curve as one moves away from the zero height, as there is for bars B1, B8, and B9. As a result, there may be no solidification on these bars from Obverse to Reverse. A scanning electron microscope was used to record the following bars at various positions on the bars, and quantitative determinations were achieved using energy-dispersed XRF analysis through intensity measurements of the element-specific wavelength.

Index Terms: Silver bars, X-ray fluorescence, Micro-X-ray fluorescence, Conductivity Meter, Scanning electron microscope

1. INTRODUCTION

Money has been used in Europe for over 2600 years to denote coined metal, particularly in the form of coins. When the term money (derived from the Middle High German "Geld") is reduced to its most fundamental meanings (replacement, compensation, value, price, retribution), all that remains is a widely accepted standard of billing, value storage, and pricing that has developed from barter. This standard is usually based on a certain amount of a coveted and durable material, often a metal, the most important raw material of antiquity. The

importance of metals is demonstrated by the fact that entire periods of history are called after them: the Copper Age (end of the Neolithic to before the 3rd century BC), the Bronze Age (before 2200 BC in Europe), and the Iron Age (before 1200 BC in Europe) (in Central Europe before 1200 BC to after 500 AD) [1]. Hence, it is not unexpected that a metal bar has been used for almost 4000 years, since the Bronze Age, as one of the original and natural forms of money (in addition to non-metallic types of money) (Fig. 1) [2].

The oldest bronze casting sites in Central Europe and Germany that have been verified to make bar bars in stone molds are in Saxony-Rotta Anhalt's and Schackstedt (evidence is available in the State Museum of Saxony-Anhalt in Halle). Since the early Bronze Age, metal bars of varying forms and weights have been used in this manner to preserve payment and value (at least verifiable from approx. 2700 BC) [4] and are also used today in many international transactions (e.g. the

Corresponding author's e-mail: Ahmad Nizamedien Barzingi, Department of Chemistry, College of Education, University of Garmian, University in Kalar, Iraq. E-mail: Ahmad.barzingi@garmian.edu.krd

method of choice for repaying national debts by switching gold bars in the Federal Reserve Bank of New York [5].

Bullion's journey can be traced throughout human history and to every corner of the globe. The ancient Egyptians utilized bar money, which was made out of precious metal rings and pieces imprinted with the Pharaoh's name. Special officials were assigned to oversee the quality and weight of silver bars in Mesopotamia during the period of Babylonian King Hammurabi (1792–1750 BC) [6]. Since silver has been in Mesopotamia since 2100 BC was the measure of value for goods, wages and prices are already in the 18th century BC a standard house for silver as a means of payment in Babylon, probably the earliest documented forerunner of DIN, known [7].

For commercial reasons, the Celts and Teutons in Northern Europe utilized standardized bronze rings and high-quality iron bars [4].

The Romans, together with the Greeks, are regarded as the forefathers of European civilization, and they utilized metal ingots as currency until approximately 200 BC [8]. The actual currency was not used until the 7th century BC, when it was developed (Fig. 2), most likely by Lydian king Alyattes II, the father of the legendary Croesus [9].

Fig. 1. Celtic pointed bars made of iron, approx. 5 kg, around 100 BC. Chr. To 100 AD. Such high-quality iron bars from the Celtic and Germanic tribes were a sought-after commodity and were mainly exported to Rome. Among other things, high-quality Roman swords were forged from it [3].

Fig. 2. Electron trite (third stater) of the Lydian king Alyattes II (approx. 613-556 BC), 4.71 g, 12 mm, enlarged illustration [3]. Alyattes was the father of Croesus and is considered the inventor of minted money [9].

Small electron bars (from Latin "electrum" = amber, signifying a natural mixture of gold and silver) were used to create the currency[10]. A seal (lion's head as the Mermnaden dynasty's coat of arms) was imprinted on the first coin's hour of birth to indicate its origin and ensure its value]. Coincidentally, about the same period, the first counterfeit coins appeared. These are lead bars that have had an electron coat applied to them (Herodotus 5th century BC). To confirm the coins' validity, they had to be sliced apart or given a deep notch, a procedure that left traces on several ancient coins that may still be seen today.

Gold and silver bars were used to replace money in Rome until the fall of the Western Roman Empire (AD 474), despite the highly established Roman currency system (Figs 4-6).

From approximately 300 AD, the Roman emperor gave legionaries a 5-year present (donative) consisting of five gold coins (aurei or solidi, Fig. 3) and a silver bar weighing one Roman pound (327, 63 g) [11].

A silver bar of this size was valued at around 200 L of wine, two annual rations of food, or about a third of the typical

Fig. 3. Solidus of the Roman Emperor Constantinus (306–337 AD), 4.56 g, 20 mm, minted around 310–313 in Trier, Fig. Enlarged (Lehmann 2010b) [3]. Flavius Valerius Constantinus, also known as Constantine the Great, introduced the solidus in 309 AD, which replaced the aureus that ran before it as a Roman imperial gold coin [10].

Fig. 4. Roman gold bar from the Munich State Coin Collection. This bar probably only represents a form of transport of the gold to the mint. The gold bar was once owned by the Swiss Federal Bank, which determines the fineness and - regardless of the art-historical value of the bar - had this stamped on the bar next to an inventory number. The fineness is 99.15%. The bar shape has been a popular shape for non-ferrous and precious metals since the Bronze Age because it made it easier to cut the bar (Photo: Lehmann).

Fig. 5. Overview of silver bars from different epochs. On the left is a Roman silver bar (target weight: 327.63 g), 7 × 10 cm), in the middle a medieval German bar (one silver mark nominally 233.856 g, 6–7 cm), on the right modern silver bar (1 kg). While you could still buy a slave for around 3 Roman bars and a small piece of land for the medieval bar, at the end of 2010 300 g of fine silver cost just under 200 euros [12].

Fig. 6. Silver bars samples.

slave price [13]. Antiquity and the Middle Ages silver bars had a radically different form and shape from today's bar silver, as seen in (Fig. 5). The double ax or skin form is seen on the Roman silver bars illustrated here [8], although most items from the German Middle Ages were shaped like a hemisphere or dome [14].

In general, X-ray fluorescence (XRF) is a non-destructive technique for the qualitative and quantitative evaluation of inorganic solids, liquids, and burned organic compounds that are based on the interaction of X-rays with matter. Cement, glass, and ceramic industries consume rocks and slag. It has become an established routine method for archaeometric investigations on precious metal objects (coins, jewelery, etc.) and other historical objects for several years, especially since

the development of transportable devices in archaeology, where it is used to quickly classify found objects and has been an established routine method for archaeometric investigations on precious metal objects (coins, jewelery, etc.). This approach is also appropriate for multi-elemental analysis of inorganic components in an organic matrix, for example to identify inorganic impurities in biological samples, only elements with an atomic number $Z > 13$ (carbon) may typically be examined [15]. More recent developments also allow the analysis of aerosols and gases.

The X-ray radiation used in XRF is electromagnetic radiation with a wavelength in the range of 0.01–10 nm and, together with the γ-rays, forms the short-wave limit range of the electromagnetic spectrum [16].

Electron microscopy enlarges pictures of things using electron beams. It is utilized for micrometer-scale surface analysis. When compared to a light microscope, accelerated electrons may attain a resolution a 1000 times >3 nm, allowing finer features to be distinguished. The device is composed of four assemblies: an electron gun, electron optics, a sample holder, and an electron detector.

When an electron beam collides with a sample surface, two types of interactions occur elastic interactions, which change the direction of the electrons without altering their energy, and inelastic interactions, which transfer the electron energies partially or entirely to the sample atoms.

Secondary electrons, Auger electrons, X-rays, heat, and light are then emitted by the excited material (electromagnetic radiation over many frequencies). Secondary electrons can be utilized to generate images [17].

The collision of an electron with an atom changes the direction of the electron but the speed and therefore the kinetic energy stays unchanged in elastic scattering. Some electrons lose their energy due to inelastic collisions and remain in the material after numerous collisions.

The majority of the energy is emitted from the surface as backscattered electrons. Secondary electrons, which are particularly crucial for image production in the scanning electron microscope (SEM), are produced in the condition of inelastic scattering. These are produced by the interaction of high-energy electrons in the beam with weakly bound electrons in the solid's conduction band, which results in the release of conduction electrons. Secondary electrons are created across the beam's interaction region with the material, but because of their low energy, they are quickly absorbed again. Only secondary electrons produced near the sample's surface can escape. Small elevations on the sample surface result in a shorter electron route length than level regions, allowing more secondary electrons to escape.

Electrical conductivity is a critical material characteristic that not only tells us how effectively a metal conducts electrical current, but also allows us to make judgments about its composition, microstructure, and mechanical capabilities.

The measurement of conductivity is based on the principle of measuring resistance. An electric current is produced in the material to be studied using a probe for this purpose, and the electrical resistance of the substance is measured. The reciprocal value of the electrical resistance determines conductivity.

$$\gamma = \frac{1}{\rho} = \frac{G}{s} = \frac{1}{R \cdot s}$$

γ: Electrical conductivity/conductivity (Sm^{-1})
ρ: The specific electrical resistance (Ω m)
G: The electrical conductance, measured in Siemens (S)
S: S: The length of Specimen measured in meters (m),
R: The resistance, measured in ohms (Ω)

2. MATERIALS AND METHODS

2.1. Conductivity Meter
The conductivity measurements were performed using a "Hocking" "AutoSigma 2000" instrument. The probe has an interior diameter of 11.5 mm and an exterior diameter of 12.5 mm, and it operates at a frequency of 60 Hz.

Conductivity measurements were used to attempt to identify the fineness and position of the flaws on the sample. The stability of the device display was verified before each measurement. A copper standard was measured 3 times before and after point measurements, and a copper standard was measured 3 times beneath plastic film, to evaluate device drift (Table 1).

2.2. SEM
XL 30, JEOL JSM-6700F Manufacturer: Philips Electronics was used for the recordings, and this has an acceleration voltage of 0.5–30 kV. The device has a secondary

TABLE 1: Stability of the measuring device

Bar money	Conductivity S/m*10⁶	Conductivity S/m*10⁶	Conductivity S/m*10⁶	Conductivity S/m*10⁶
	Average 1	Average 2	Average - Foil 1	Average -Foil 2
B8 (Obvers)	58.6	58.567	58.3	58.4
B8 (Revers)	58.63	58.63	58.3	58.367
B2 (Obvers)	58.7	58.71	58.367	58.367
B2 (Reverse)	58.667	58.7	58.33	58.366

electron detector, backscattered electron detector, Si (Li) semiconductor detector as a detector.

2.3. XRF Spectroscopy

The measurements with µ-XRF analysis aimed to determine the fineness and the components of the bars B1, B2, B3, B4, B6, B8, B9, B10, BT1, BT3, BT6 (Table 2).

The "Eagle µ-Probe II" device from EDAX was used for the measurement. The device has an X-ray tube with a beryllium window, rhodium target, an acceleration voltage of 10–40 keV, a cathode current of 40–1000 µA and a Si (Li) detector was used as a detector.

3. RESULTS AND DISCUSSION

3.1. Conductivity Measurement

The conductivity of the following bars was measured: B1, B2, B3, B4, B5, B6, B8, B9, B10, BT1, BT3, BT6. (Fig. 6). Because

TABLE 2: Silver bars description in term of weight and dimension

| No.	Weight (g)	Dimension (cm)
B1	191.4	5.9×1.2
B2	187.5	6×1.1
B3	246.3150	6.3×1.09
B4	249.149	6.7×1.2
B5	187.232	
B6	197.2456	5.8×1.3
B8	211.790	6.1×1.1
B9	132.0670	6.4×1.2
B10	128.876	5.3×1.08
BT1	71.165	
BT3	64.317	
BT6	62.835	

TABLE 3: Conductivity of the bars with standard deviation (σ)

		Conductivity (S/m *10⁶)			
No.	Bars	Obvers	Revers	σ (Obvers)	σ (Revers)
1	B1	16.05	10.41	2.45	1.98
2	B2	13.16	10.07	2.85	3.15
3	B3	40.51	33.95	3.25	1.9
4	B4	16.14	11.73	1.47	1.67
5	B5	20.03	12.69	0.75	1.84
6	B6	20.34	14.63	1.27	2.45
7	B8	15.46	12.5	1.06	3.39
8	B9	23.87	18.98	1.13	2.87
9	B10	36.96	24.76	5.19	0.40
10	BT1	20.40	13.89	0.53	2.23
11	BT3	20.06	11.27	0.29	2.37
12	BT6	21.65	18.06	0.19	5.41

unevenness affects conductivity, the tests were taken on the flattest areas of the bars. On each sample, 10 points on the front and 10 points on the reverse were chosen. Because of unbalancing, several samples could not be measured to 10 points. The conductivity was measured on all 10 silver bars. The detailed measurement results can be found in Table 3. The values fluctuate within the error limits specified by the device manufacturer of ± 0.1 MS/m at room temperature.

Fig. 7 shows wave-like fluctuations in the conductivity of the bars. There are some bars such as B3 and B9; these bars have a higher conductivity than the rest. This is perhaps due to the silver content of the bars.

The average conductivity of the obverse is 22.05 ± 1.70 and the reverse 16.07 ± 2.47 MS/m. As can be seen from the results, avers has a higher conductivity than the reverse. That means the obverse has a higher fineness than the reverse. This is proof that the bars slowly solidified from the obverse so that segregation has occurred (Fig. 8).

There is a 5.98 MS/m average conductivity difference between the front and back. This discrepancy might be
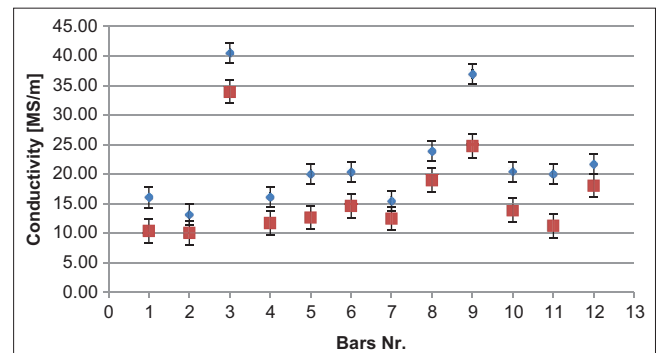
Fig. 7. Average conductivities on the obverse and lapel. ◆ Blue conductivity of the obverse (MS/m), ■ Red Conductivity of the revers (MS/m).
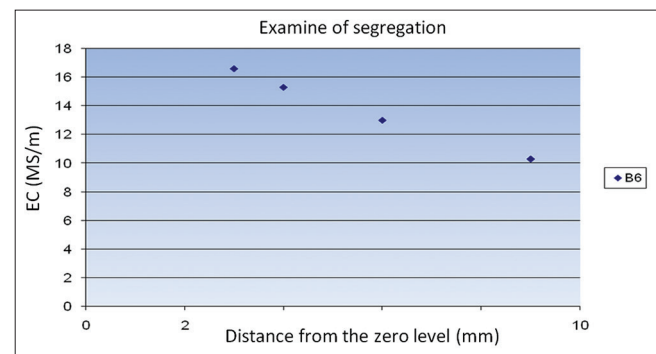
Fig. 8. Conductivity curve on the bar 6.

produced by a variety of factors, including device limitations, corrosion layers, and fineness changes from front to back, such as more silver on the front than the opposite.

The segregation of the bars was investigated. The technique of separating distinct items in an observation area is referred to as segregation. A zero level was established on the bars for this reason. The transition from obverse to reverse was specified at the zero levels. Segregation on the bars can be noticed if the conductivity diminishes proportionately to the distance from the zero levels.

All bars were subjected to the segregation test. It was not feasible to prove that segregation had occurred in the case of certain bears. There is no decreasing conductivity curve as one moves away from the zero height, as there is for bars B1, B8, and B9. This might result in no solidification on these bars from the Avers to the Revers.

Influence of the stamps on the conductivity (EC);

The influence of the stamps on the conductivity was investigated. According to the theory, the stamping should result in lower conductivity. The results are shown in Table 4.

According to theory, stamping should result in lower EC, but this difference does not seem to be significant, that is, on the Revers, segregation is probably the main cause of the various EC.

3.2. Measurements by the SEM

The goal is to learn about the equipment and how to utilize SEM, as well as to learn about the surface characteristics of the bars. A SEM was used to record the following bars at various positions on the bars, and quantitative determinations were achieved using energy-dispersed X-ray fluorescence analysis (EDX) through intensity measurements element-specific wavelength (Fig. 9).

For image B3-05, EDX was made on a wise matrix, on points and dark points (Fig. 10).

The results are given in the table below.

In Table 5, it is clear that the dark points are predominantly made of carbon. The Cl content determined whether the salts have formed on the surface of the bar, but it cannot be clearly stated that the salts have formed because the Cl content is too small.

With the SEM-EDX, light elements such as carbon and oxygen were detected compared to the μ-XRF

Image B5-01 was taken to determine whether the drawings can be recognized as writing. The drawings suggest the scriptures to some extent (Fig. 11).

An attempt was made in image B5-08 to clarify whether or not it is a "M" letter. However, it is not as obvious (Fig. 12).

3.3. XRF Analysis

The measurements with μ-XRF analysis aimed to determine the fineness and the components of the bars B1, B2, B3, B4, B6, B8, B9, B10, BT1, BT3, BT6.

The "Eagle μ-Probe II" device from EDAX was used for the measurement. The device has an X-ray tube with a beryllium window, rhodium target, an acceleration voltage of 10 to 40 keV, a cathode current of 40 to 1000 μA and a Si (Li) detector was used as a detector.

For each bar, 20 points were placed on the obverse and 20 points on the reverse, resulting in a generally circular form. Table 6 shows the corrected findings after adding the standards to the basic parameter correction. Silver

TABLE 4: Conductivity values with and without stamps, with the picture punch element-specific wavelength. B3 bar with different photos

Bars	EC without stamps	EC with stamp1	EC with stamp 2	EC with stamp 3	Picture punch 1	Picture punch 2	Picture punch 1
B6	20.8	21.8	19.9		Star	Lion	
B8	13.7	16.3	16.9		Head	Lion	
B3	36.4	32.3			Sign		
B2	14.1	16.4	14.4	7.9	Crown	D.	Lion (crack)
B9	24.8	24.1	24.6	24.6	Flower	W.	?
B1	14.3	17.6	18.8		Lion	Star	
B4	16.4	18.6	18.5		Lion	Flowe	
BT1	20.6	19.9			Lion		
B10	33.8	34.8			Lion		
B5	21.4	18.8			?		
BT3	20.3	19.3			Pikas		

TABLE 5: The chemical composition of B3-05

Elements	Wise Matrix	Point	Dark structure
C %	6,5	44	38
O %	1.2	8	8
Cl %	0.6	0.1	2
Ag %	88.6	4	45
Cu %	0.7	36	1
Pb %	2.3	6	5

was found as the major component in all twelve bars, with copper and lead as minor components. The bars contain a silver composition of 6.49 4.07 percent by weight copper and 6.38 3.28 percent by weight lead, with an average of 87.63 5.86 percent by weight. There are extremely high standard variations with an average copper and lead concentration. This demonstrates how the copper and lead contents of each ingot vary greatly. The silver content has

TABLE 6: Measuring the weight percentage of silver bar samples by µ-XRF of both sides

Sample ID	Side	Obverse	AgK	AgL	Cu	Pb
B1	Obv.	Average	85.944	87.013	7.779	6.278
		STD	3.179	3.057	2.451	1.981
	Rev.	Average	77.239	78.268	10.103	12.659
		STD.	2.269	6.135	1.471	3.091
B2	Obv.	Average	81.678	89.595	13.085	5.237
		STD	6.739	2.613	4.287	4.218
	Rev.	Average	89.922	88.340	4.295	5.737
		STD	3.154	3.997	1.824	2.135
B3	Obv.	Average	89.786	94.151	5.637	3.635
		STD	4.201	2.342	2.509	2.482
	Rev.	Average	96.593	96.264	2.014	1.395
		STD	1.829	2.042	0.639	1.742
B4	Obv.	Average	82.717	89.601	8.261	9.024
		STD	4.854	3.715	1.481	5.440
	Rev.	Average	85.966	85.995	4.746	9.289
		STD	4.507	3.457	1.430	4.324
B5	Obv.	Average	87.367	88.984	4.289	5.345
		STD	3.321	3.324	1.547	2.768
	Rev.	Average	88.462	89.664	5.915	5.622
		STD	3.718	3.177	1.585	2.853
B6	Obv.	Average	81.312	88.461	9.256	9.331
		STD	4.501	3.226	1.987	3.286
	Rev.	Average	91.031	92.098	5.110	3.853
		STD	4.520	3.465	1.537	3.085
B8	Obv.	Average	87.359	90.729	6.040	6.601
		STD	6.388	3.862	3.734	4.317
	Rev.	Average	91.333	90.635	2.875	5.793
		STD	2.747	4.778	0.936	2.864
B9	Obv.	Average	94.835	95.275	1.867	3.297
		STD	1.210	0.765	0.352	1.163
	Rev.	Average	93.847	93.689	2.809	3.316
		STD	3.089	3.438	0.379	3.056
B10	Obv.	Average	96.265	91.511	1.557	2.179
		STD	1.657	2.534	0.555	1.195
	Rev.	Average	94.539	94.794	2.404	3.057
		STD	3.129	4.005	0.665	3.452
BT1	Obv.	Average	90.301	89.729	5.359	5.495
		STD	4.167	4.914	3.538	3.356
	Rev.	Average	90.430	82.873	4.869	5.273
		STD	4.351	28.147	1.510	3.958
BT3	Obv.	Average	75.150	77.330	13.250	11.610
		STD	8.160	5.540	7.690	3.590
	Rev.	Average	69.948	83.247	15.648	13.300
		STD	4.708	3.152	3.581	3.668
BT6	Obv.	Average	89.701	89.433	4.892	5.408
		STD	4.233	4.187	2.112	2.533
	Rev.	Average	75.963	88.397	13.644	10.393
		STD	10.026	3.254	4.820	7.771

the highest B9 bar, with an approximate value of the copper and lead content have the maximum BT3 bar, with around 95.14 percent and 12 percent, respectively.

The iron and gold composition of the bar could be determined. That was not accomplished in our effort. Table 7 shows the ratio of the intensities of the generated Ag-K and Ag-L signals to determine the thickness of the corrosion layer.

According to the AgK/AgL ratios, the obverse of all Roman bars has a slightly thicker corrosion layer than the reverse. This might be owing to a site-specific storage facility in the earth or other unique features.
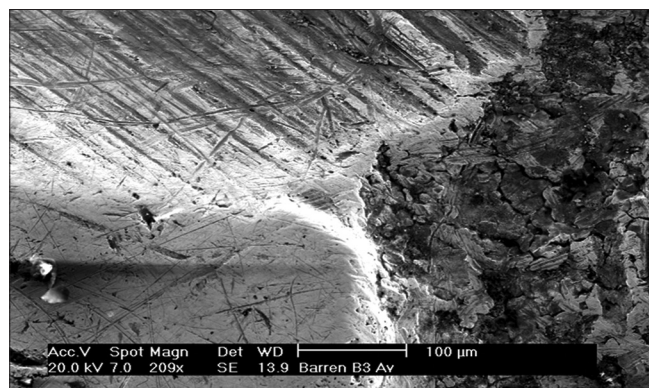
4. CONCLUSION

The conductivity of the bars is shown by wave-like variations. The conductivity of the B3 and B9 is greater than that of the others. This is because the bars contain silver.

The average conductivity of the obverse is 22.05 ± 1.70 and the reverse 16.07 ± 2.47 MS/m. Obvers has a higher conductivity than the reverse. That means obverse has a higher fineness than revers. This is proof that the bars have slowly solidified from the obverse so that segregation has occurred.

TABLE 7: AgK/AgL ratio of difference silver bars

	*AgK/AgL Ratio					
	B1	B2	B3	B4	B5	B6
Obvers	0.088	0.081	0.075	0.092	0.098	0.091
Revers	0.098	0.090	0.088	0.097	0.099	0.094
	B8	B9	B10	BT1	BT3	BT6
Obvers	0.076	0.074	0.085	0.096	0.077	0.071
Reverse	0.094	0.079	0.099	0.010	0.084	0.085

The peak intensities of AgK and AgL line are measured as cps/eV[18]

All bars were subjected to the segregation test. In the instance of certain bars, it was not always feasible to state unequivocally that segregation had happened. There is no diminishing conductivity curve as one moves away from the zero height, as there is for bars B1, B8, and B9. As a result, there may be no solidification on these bars from obvers to reveres.

A SEM was used to record the following bars at various positions on the bars, and quantitative determinations were achieved using EDX through intensity measurements of the element-specific wavelength.

The measurements with μ-XRF analysis aimed to determine the fineness and the components of the bars B1, B2, B3, B4, B6, B8, B9, B10, BT1, BT3, BT6.

For each bar, 20 points were placed on the obverse and 20 points on the reveres, resulting in a generally circular form. In all twelve bars, silver was identified as the main component and copper and lead as the minor component. With an average of $87.63 \pm 5.86\%$ by weight, the bars have a silver content of $6.49 \pm 4.07\%$ by weight copper and $6.38 \pm 3.28\%$ by weight lead. With an average copper and lead content, there are very large standard deviations.
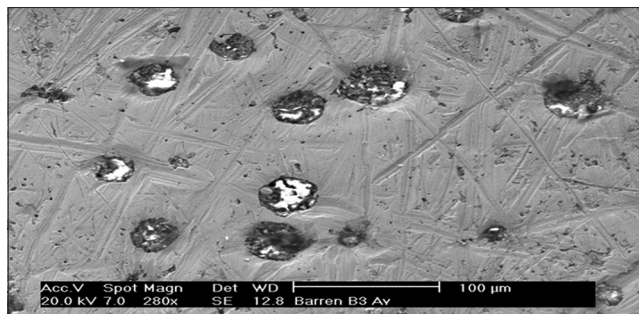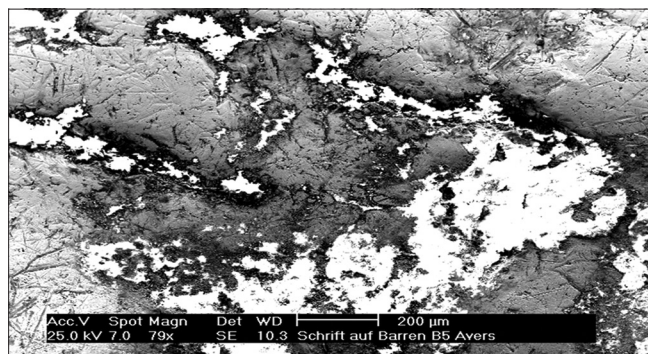

Fig. 10. Image B3-05: The obverse image of round inclusions [18].

Fig. 9. Image B3-01: Photo at the point where is the casting-demolition transition.
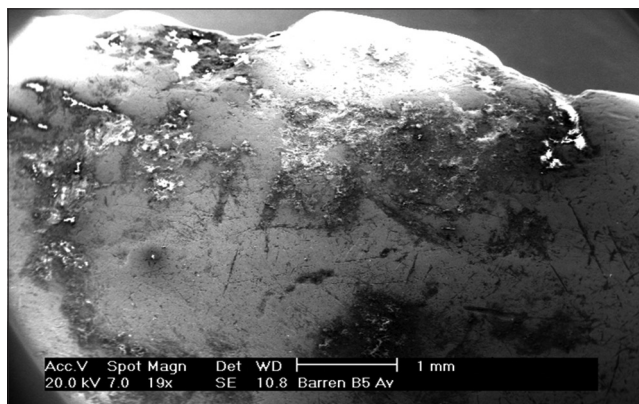
Fig. 11. Image B5-01: Photo of bar B5.

Fig. 12. Image B5-08: Writing on obverse B5 bar.

This shows that the copper and lead contents of each ingot vary widely. The silver content has the highest B9 bar with approx. 95%, the copper and lead content have the highest BT3 bar with approx. 14% and 12%. The iron and gold composition of the bar may be analyzed. That was not done in our work. According to the AgK/AgL ratios, the reverse of all silver bars (B1, B2, B3, B4, B5, and B6) has a somewhat thicker corrosion layer than the face. This might be owing to a location-specific storage facility in the earth or other particular properties.

REFERENCES

[1] H. J. Eggers. "Zur Absoluten Chronologie der römischen Kaiserzeit im Freien Germanien". In: *Aufstieg u. Niedergang röm. Welt II*, pp. 3-6, 1976.

[2] M. Pfefferkorn. "*Seit 4000 Jahren Zahlungsmittel, Vorstufen des Münzgeldes-Vom Bronzebarren Zum Goldenen Oban, Moneytrend*", vol. 9, pp. 118-122, 2003.

[3] R. Lehmann. *"Barren versus Münze, Teil I: Barrengeld Damals Und Heute Und Die Besondere Bedeutung im Mittelalter, Moneytrend"*, vol. 10, pp. 134-139, 2010b.

[4] T. Lautz. *"Barren als Zahlungsmittel. Von der Bronzezeit Bis Ins 20. Jahrhundert, Das Fenster in der Kreissparkasse Köln, Thema 163, Köln"*, 2003.

[5] A. Anikin. *"Gold, Verlag Die Wirtschaft, Berlin"*, pp. 77-80, 1982.

[6] K. Reiter. *"Die Metalle im Alten Orient unter besonderer Berücksichtigung Altbabylonischer Quellen, Ugarit-Verlag, Münster"*, pp. 43, 47, 83-103, 113, 289, 299-305, 401, 405-415, 425, 435-437, 452, 455, 1997.

[7] K. Volke. *"Zu den Anfängen der Analytischen Chemie: Wider Fälscher und Betrüger, Chemie in unserer Zeit"*. 4th ed. WILEY-VCH Verlag, Weinheim, pp. 268-275, 2004.

[8] R. Wiegels. *"Silberbarren der Römischen Kaiserzeit, Katalog und Versuch Einer Deutung, Freiberger Beiträge zur Archäologie und Geschichte des Ersten Jahrtausends, Rahden/Westf"*, 2004.

[9] L. Biosas. *"Griechische Münzen, Faszination und Geschichte, Numismatischer Verlag Fritz Rudolf Künker, Osnabrück"*, pp. 493-504, 2005.

[10] F. Schrötter. "*Wörterbuch der Münzkunde, de Gruyter Verlag, Berlin",* 1930.

[11] B. Kluge. "*Die Monetarisierung Europas in Staufischer Zeit, Numismatisches Nachrichtenblatt (NNB), 09/2010, 14150*", pp. 325-331, 2010.

[12] R. Lehmann and C. Vogt, C. "*Wer Den Pfennig nicht Ehrt Ist Die Mark Nicht Wert?*" 2010a.

[13] "*W. Szaivert-R. Wolters, Löhne, Preise*", 2005. Available from: https://www.w.pd.file:///e:/research2021/xrf&sem/referances/"no title. [Last accessed on 2021 Nov 12].

[14] A. Loehr. "*Probleme der Silberbarren, Numismatische Zeitschrift, Wien*", vol. 24, pp. 101-109, 1931.

[15] H. Ehrhardt. "*Röntgenfluoreszenzanalyse-Anwendung in Betriebslaboratorien*". 2nd ed. Springer-Verlag, Berlin, 1989.

[16] C. Vogt. "*Skript zur Vorlesung, Grundlagen der Analytik I, Röntgenspektroskopie, Universität Hannover",* 2006.

[17] A. Feldhoff, 2007. Available from: https://www.notitlefile:///f:/localdisk/analytikvorlesungungen.vogt/fortgeschrittenematerialanalytik/materialanalytik-i-2007-feldhoff.pdf. [Last accessed on 2021 Oct 11].

[18] S. M. M. Hrnjić, G. A. Hagen-Peter, T. Birch, G. H. Barfod, S. Sindbæk and C. E. Lesher. "*No Title Non-Destructive Identification of Surface Enrichment and Trace Element Fractionation 4 in Ancient Silver Coins*", 2020.